

RESEARCH ARTICLE

10.1002/2014JA020016

Key Points:

- We provide new insights on L^*
- We derive a new analytical approximation for L^*
- No drift shell tracing nor iterative search algorithm is required

Correspondence to:

S. Lejosne,
solene.lejosne@yahoo.fr

Citation:

Lejosne, S. (2014), An algorithm for approximating the L^* invariant coordinate from the real-time tracing of one magnetic field line between mirror points, *J. Geophys. Res. Space Physics*, 119, 6405–6416, doi:10.1002/2014JA020016.

Received 26 MAR 2014

Accepted 30 JUL 2014

Accepted article online 4 AUG 2014

Published online 22 AUG 2014

Corrected 22 SEPT 2014

This article was corrected on 22 SEPT 2014. See the end of the full text for details.

An algorithm for approximating the L^* invariant coordinate from the real-time tracing of one magnetic field line between mirror points

Solène Lejosne^{1,2}

¹British Antarctic Survey, Natural Environment Research Council, Cambridge, UK, ²Now at Space Sciences Laboratory, University of California, Berkeley, California, USA

Abstract The L^* invariant coordinate depends on the global electromagnetic field topology at a given instance, and the standard method for its determination requires a computationally expensive drift contour tracing. This fact makes L^* a cumbersome parameter to handle. In this paper, we provide new insights on the L^* parameter, and we introduce an algorithm for an L^* approximation that only requires the real-time tracing of one magnetic field line between mirror points. This approximation is based on the description of the variation of the magnetic field mirror intensity after an adiabatic dipolarization, i.e., after the nondipolar components of a magnetic field have been turned off with a characteristic time very long in comparison with the particles' drift periods. The corresponding magnetic field topological variations are deduced, assuming that the field line foot points remain rooted in the Earth's surface, and the drift average operator is replaced with a computationally cheaper circular average operator. The algorithm results in a relative difference of a maximum of 12% between the approximate L^* and the output obtained using the International Radiation Belt Environment Modeling library, in the case of the Tsyganenko 89 model for the external magnetic field (T89). This margin of error is similar to the margin of error due to small deviations between different magnetic field models at geostationary orbit. This approximate L^* algorithm represents therefore a reasonable compromise between computational speed and accuracy of particular interest for real-time space weather forecast purposes.

1. Introduction

Orbiting within or through the hazardous environment of Earth's radiation belts, spacecraft are prone to failures of various types and durations [Bedingfield *et al.*, 1996]. The consequences of these failures range from minor damage to the electronics to the loss of all spacecraft functions and the premature ending of the mission [Koons *et al.*, 2000]. To better understand the Earth's radiation belts and thereby help develop strategies to minimize deleterious effects on related economic and societal stakes [National Research Council, 2008], dedicated space probes are launched, and more sophisticated theoretical models are developed. The objective of this collective effort is to enhance the understanding of the drivers of the radiation belt dynamics, i.e., the understanding of particle injection, transport, acceleration, and loss processes. Particular attention is paid to generate operational tools in order to forecast the effects of space weather [e.g., Horne *et al.*, 2013].

Computer codes to model the dynamics of the Earth's radiation belts such as the Salammbô model at ONERA [e.g., Beutier and Boscher, 1995] or the British Antarctic Survey radiation belt model [Glauert *et al.*, 2013] rely on adiabatic invariant theory and statistics to reduce the number of variables to handle and ultimately to optimize the execution time of the codes. Based on adiabatic invariant theory, the dynamics is averaged over the higher frequencies of the particle quasiperiodic motions in order to work with time steps that are consistent with the size of the time interval to model. Rather than focusing on the dynamics of individual particles, they use distribution functions relating directly to measurements [e.g., Roederer and Zhang, 2014].

Accordingly, data are binned as a function of the three invariant coordinates (M, J, Φ), or preferably (M, K, L^*), an equivalent choice when assuming the absence of external forces parallel to the magnetic field [e.g., Roederer, 1970]. These invariant coordinates characterize the magnitude of the three periodic motions of the radiation belt population: gyration perpendicular to the magnetic field direction (M), bounce motion along the magnetic field line between the mirror points (J or K in the absence of parallel forces), and drift motion around the

Earth (Φ or equivalently L^*). L^* is responsible for organizing data in radial distance; therefore, deriving L^* from spatial coordinates is a key step toward understanding and forecasting radiation belt dynamics [Yu *et al.*, 2012].

L^* is a dimensionless quantity introduced by Roederer [1970] according to the equation

$$L^* = \frac{2\pi k_0}{\Phi R_e}, \quad (1)$$

where k_0 is the magnetic moment of the Earth's dipole and Φ is the third adiabatic invariant in absolute values. $\Phi = \iint B(r, t) \cdot dS$ corresponds to the magnetic flux delimited by the guiding drift shell of a radiation belt population at a given time t . When defining the guiding drift shell, the effects of electrostatic potentials are commonly omitted. In addition, since measurements cannot give the global magnetic field at a given instance, a suitable magnetic field model is required. From the given magnetic field model, the standard method of calculating L^* consists of two steps [Roederer, 1970]: first, an iterative search for the field lines with the same first two adiabatic invariants as the radiation belt population considered is performed; then, the magnetic flux Φ is integrated over the polar cap region bounded by the intersection of the field lines with the Earth's surface. This procedure is implemented for example by the Fortran Library International Radiation Belt Environment Modeling (IRBEM) [Boscher *et al.*, 2012]. However, since this technique is computationally expensive, it is highly desirable to have a faster method of calculating L^* , particularly for use in real-time forecasting models.

For rapid L^* calculations, two main approaches have been taken. First, Koller *et al.* [2009] and Koller and Zaharia [2011] developed an artificial neural network called LANL* that enables a drastic increase in speed of almost 6 orders of magnitude compared to the conventional method while maintaining accuracy. However, the approach is not physics based, and it requires substantial training and validation whenever a new magnetic field model is introduced, which may be quite unwieldy. Second, Min *et al.* [2013a, 2013b] suggested a physics-based method which consists of determining possible drift trajectories using the principle of energy conservation and integrating the magnetic flux Φ over the polar cap region bounded by the intersection of the shell field lines with the Earth's surface. As mentioned by the authors, the approach is essentially an extension of Roederer's [1970] standard technique, which prevents the propagation of errors with time with a possible inherent limit due to the use of a two-dimensional finite grid.

While excellent accuracy is a main result for both approaches, it has been proven that even small differences between magnetic field models lead to significant variations between the calculated L^* . Huang *et al.* [2008], for example, mentioned that L^* computed at geosynchronous orbit varies by $\sim 13\%$ between T96 [Tsyganenko, 1995] and TS05 [Tsyganenko and Sitnov, 2005]. McCollough *et al.* [2008] noted that a 2% difference between magnetic field models could generate as much as a 10% difference between the resulting L^* . The accuracy with which L^* reliably organizes data is a function of the accuracy with which the global electromagnetic topology is reliably rendered at a given instance. However, the modeling of the geomagnetic field is the object of constant improving [e.g., Tsyganenko and Sitnov, 2007], and the effects of electrostatic potentials on the distortion of the particles' drift shells are currently still disregarded [e.g., Min *et al.*, 2013a]. Due to these existing limitations, maintaining excellent accuracy when computing L^* should not necessarily be a prime concern. A coarser L^* approximation with a margin of error similar to the margin of error induced by small deviations between magnetic models, for example, can still provide valuable information regarding radiation belt dynamics while benefiting from being fast and accessible. We believe that the algorithm proposed in this paper represents such a compromise.

Section 2 details the theoretical framework of the study and provides new insights on the L^* parameter. Section 3 describes the derivation of the L^* approximation used. Section 4 presents the algorithm for the approximate L^* computation and discusses its performance in the case of the T89 external magnetic field model [Tsyganenko, 1989].

2. Theoretical Framework

We assume that the three adiabatic invariants are defined and conserved when determining L^* . Accordingly, regions affected by drift orbit bifurcations [e.g., Ukhorskiy *et al.*, 2014] are not considered. We assume also that the energy range of the radiation belt particles considered is such that electrostatic potentials can be

neglected (i.e., $\geq \sim 100$ keV, [e.g., Schulz, 1991]). Since the derivation given in section 3 relies on the tracking of a drift trajectory after an adiabatic dipolarization, i.e., after the nondipolar components of the magnetic field have been turned off with a characteristic time very long in comparison with the particles' drift periods, we first focus on characterizing a drift trajectory in the limiting case of a static magnetic field.

2.1. Modeling Drift Trajectories in a Static Magnetic Field

When the magnetic field is static, in the absence of external forces, radiation belt particles drift on closed shells, and the mirror field intensity B_m is an invariant of the drift motion. Therefore, the intersection of a shell with the minimum B surface defines a closed curve, called the guiding drift contour Γ , characterized by the relation

$$\forall (\mathbf{r}, \mathbf{r}_0) \in \Gamma, B_m(\mathbf{r}) = B_m(\mathbf{r}_0), \quad (2)$$

where B_m is the magnetic field intensity at the magnetic mirror point [e.g., Whipple, 1978]. The tracing of a guiding drift contour related to a given radiation belt population does not depend on the population charge, mass, or energy. It depends on the azimuthal variations of the magnetic field topology, i.e., on the azimuthal asymmetry of the magnetic field. In a symmetric magnetic field, the guiding drift contour is a circle; moreover, in that case, particles starting on the same field line with different equatorial pitch angles populate the same drift shell. They share the same guiding drift contour, and as a result, they have the same L^* coordinate. This degeneracy is broken by the asymmetry of the magnetic field which generates noncircular guiding drift contours and drift shell splitting [e.g., Roederer, 1967]. In a weakly asymmetric magnetic field model in which the asymmetric component is only a small perturbation, Roederer [1972] and Schulz [1972] have described analytically the guiding drift contours and the extent of the shell splitting effect. They have shown that guiding drift contours are off-center circles. The radius r_0 corresponds to the distance of the magnetic equator of the field line to the position of the Earth's internal dipole. The offset is proportional to the azimuthal asymmetry of the magnetic field weighted by a coefficient characterizing the shell splitting effect. According to the approximation given by Schulz [1972; equations (25), (26a), and (26b)], this shell splitting coefficient ranges continuously from -0.33 (equation (26b)) to 0.15 (equation (26a)) as the equatorial pitch angle of the population $\alpha \equiv \sin^{-1} y$ decreases from 90° ($y = 1$) to 0° ($y = 0$).

In a dipole magnetic field, $\Phi = 2\pi k_0/r_0$ and following the definition given in equation (1), L^* is simply the radius of the circular guiding drift contour in units of Earth radii (in what follows, any radius will be expressed in units of Earth radii). This identification is not possible in magnetic field topologies other than the dipole. However, since L^* is an adiabatic invariant, L^* is the radius of the circular guiding drift contour on which particles are found after we have turned off adiabatically all nondipolar contributions to the magnetic field [Roederer, 1970].

2.2. Magnetic Field Dipolarization

As the time variation of the magnetic field is turned on, a rotational electric field is set up according to Faraday's law. We consider that $\mathbf{E} \cdot \mathbf{B} = 0$ [e.g., Stern, 1994]. In addition, we assume that the Earth's surface is a perfectly conducting surface. Accordingly, the time-varying magnetic field topology has its field line foot points rooted in the Earth's surface, and the local magnetic field line velocity coincides with the local $\mathbf{E} \times \mathbf{B}$ drift velocity [e.g., Birmingham and Jones, 1968; Fälthammar and Mozer, 2007]. We consider therefore that the position of a field line foot point only depends on the internal magnetic field chosen. We select the internal dipole magnetic field for that purpose. To this constant internal field, we superimpose a given time-dependent external magnetic field model. We can then retrieve the equatorial position of any closed field line after a dipolarization by considering only the computed position of the field line foot point.

To retrieve this equatorial dipolar position, we trace a field line in a given magnetic field model, we compute the position of the foot point $(1, \theta_e, \varphi_e)$, and we apply at $(1, \theta_e, \varphi_e)$ the equation of a dipolar magnetic field line

$$\frac{r}{\sin^2 \theta} = L^*. \quad (3)$$

We deduce that the equatorial radius of the field line after a dipolarization L_{dip}^* is given by

$$L_{\text{dip}}^* = \frac{1}{\sin^2 \theta_e}. \quad (4)$$

L_{dip}^* is similar to the parameter introduced by Schulz [1972] according to the relation $L_d \equiv \lim_{\theta \rightarrow 0} (r / \sin^2 \theta)$.

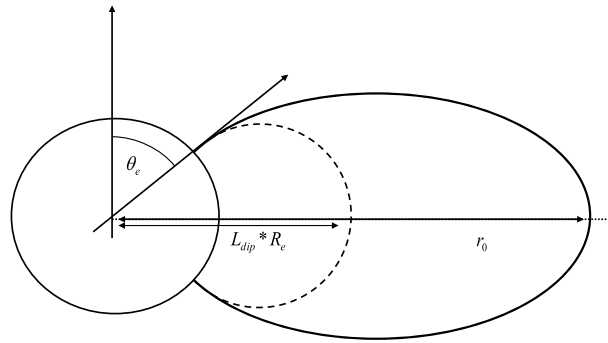


Figure 1. The $L_{dip}^* R_e$ parameter.

We obtain information regarding the motion of a field line due to dipolarization by comparing L_{dip}^* with the distance of the current magnetic equator r_0 (Figure 1). In addition, since the $\mathbf{E} \times \mathbf{B}$ drift is flux preserving [e.g., Newcomb, 1958], the flux through the minimum B surface delimited by a bunch of magnetic field lines circling the Earth in a given magnetic field instance equals the flux through the minimum B surface delimited by the same field lines after

dipolarization. In other words, if we assume that this initial bunch of field lines circling the Earth defines a drift shell characterized by L^* , with the definition given equation (1) and the magnetic flux in a dipole taken at the minimum B surface given by $\Phi = \oint k_0 d\varphi / r R_e$, we have

$$\frac{2\pi k_0}{L^* R_e} = \oint \frac{k_0 d\varphi}{L_{dip}^*(\varphi) R_e}, \tag{5}$$

i.e.,

$$\frac{1}{L^*} = \frac{1}{2\pi} \oint \frac{d\varphi}{L_{dip}^*(\varphi)}. \tag{6}$$

We now relate these field line mapping properties to the tracking of particle drift motions after dipolarization.

2.3. Variation of the Radial Drift Motion in the Case of a Magnetic Field Dipolarization

In a time-varying magnetic field, energy is imparted to the particles by means of the curl of \mathbf{E} which acts around the gyration circles (gyrobetatron) and the drift contours (drift betatron) [Fillius and McIlwain, 1967]. Accordingly, the particles' mirror field intensity is not a constant of the drift motion anymore. The tracing of the drift motion of a particle depends on the competition between the characteristic time for the variation of the field and the drift period. When the characteristic time for the variation of the field is very fast in comparison with the drift period, the $\mathbf{E} \times \mathbf{B}$ drift velocity dominates the magnetic drift velocity. In the limiting case of a "zero magnetic drift velocity," the particle remains attached to the magnetic field line since the $\mathbf{E} \times \mathbf{B}$ drift coincides with the local magnetic field line velocity [e.g., Roederer, 1970]. The equatorial radial position of the particle varies from r_0 initially to L_{dip}^* after a very fast dipolarization. This radial motion may lead to the violation of the L^* invariant coordinate since L_{dip}^* does not necessarily equals the initial L^* . In the opposite case of a magnetic field which varies adiabatically, the drifting particle scans all the field lines of the guiding drift contour at each time step of the magnetic field variation, and L^* is preserved. After the adiabatic dipolarization, the equatorial radial position of this drifting particle L^* falls from equation (6). We define the drift average operator $f \mapsto \langle f \rangle$ according to the equation

$$\langle f \rangle = \frac{1}{2\pi} \oint_{\Gamma} f(\mathbf{r}, \varphi) d\varphi \tag{7}$$

with the integration performed along the guiding contour Γ . Equation (6) becomes

$$\frac{1}{L^*} = \left\langle \frac{1}{L_{dip}^*} \right\rangle. \tag{8}$$

The equatorial radial position of the drifting particle L^* is the harmonic drift average of the L_{dip}^* parameters of the field lines constituting the initial drift shell. Additionally, we retrieve the equation (3.40) given by Roederer and Zhang [2014, p. 83] by putting equation (4) into equation (8)

$$L^* = \frac{1}{\langle \sin^2 \theta_e \rangle}. \tag{9}$$

$\langle 1/L_{dip}^* \rangle = 1/L_{dip}^*$ in the case of a symmetric magnetic field. In an asymmetric time-varying magnetic field, a particle does not necessarily remain attached to the bunch of magnetic field lines $L_{dip}^*(\varphi)_{\varphi \in [0, 2\pi]}$

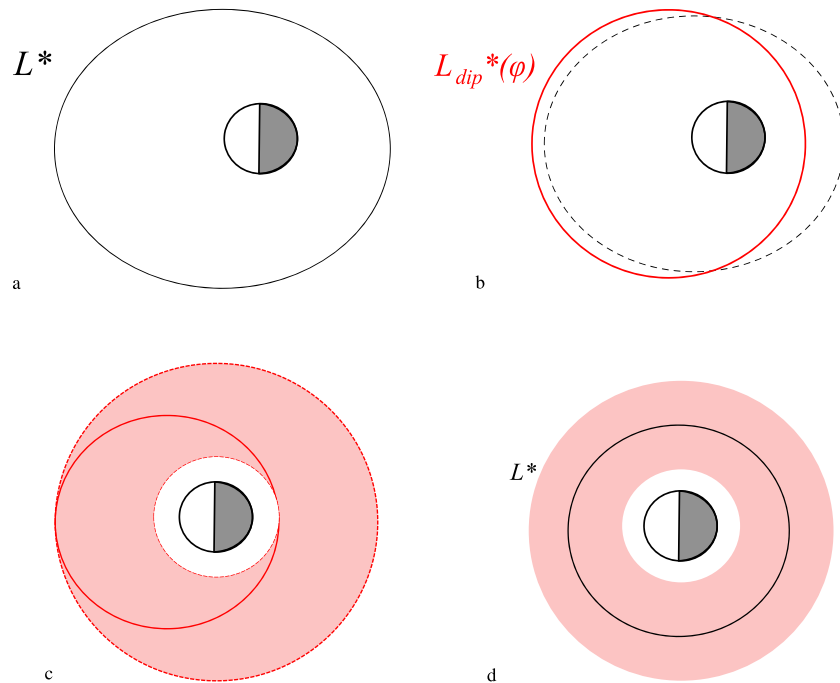


Figure 2. (a) A guiding drift contour in an asymmetric magnetic field corresponding to an L^* parameter. (b) Equatorial positions of the dipolar field lines initially constituting the drift shell $L_{dip}^*(\varphi)R_e$. (c) Area generated by the (circular) guiding drift contours intersecting the dipolar field lines initially constituting the drift shell. (d) The dipolar guiding drift contour corresponding to the initial L^* parameter.

constituting its initial drift shell; equivalently, a bunch of field lines constituting a drift shell for a population at a given time does not necessarily constitute a drift shell for the same population at a later time. For example, we represent a guiding drift contour relative to equatorial particles drifting in an asymmetric magnetic field in Figure 2a. This contour corresponds to one L^* parameter. Since field lines are generally compressed on the dayside and stretched on the nightside, the magnetic field intensity is generally stronger on the dayside at the minimum B surface for a given radius. Consequently, the guiding drift contour has its closest approach to the Earth on the nightside. In addition, because fields lines are compressed on the dayside and stretched on the nightside, the equatorial positions of the field lines intersecting the guiding drift contour move inward on the nightside and outward on the dayside during dipolarization. Their positions after dipolarization $L_{dip}^*(\varphi)_{\varphi \in [0, 2\pi]}$ are sketched in red in Figure 2b. Since the curve constituted by these $L_{dip}^*(\varphi)_{\varphi \in [0, 2\pi]}$ positions is not circular, it cannot be a guiding drift contour in the dipole. In Figure 2c, we represent in light red the surface generated by all the possible guiding drift contours $L_{dip}^*(\varphi)_{\varphi \in [0, 2\pi]}$. In Figure 2d, we represent the harmonic drift average L^* , following equation (6). This contour corresponds to the shell where equatorial particles end up after an adiabatic dipolarization. In the opposite limiting case of a very fast dipolarization, particles end up populating the shells generated by the $L_{dip}^*(\varphi)_{\varphi \in [0, 2\pi]}$ family as they resume their magnetic drift motions (in light red in Figure 2d). Their L^* coordinates vary depending on the longitude according to the relation $\Delta L^*(\varphi) = L_{dip}^*(\varphi) - L^*$. Equation (5) shows that the variation of the population magnetic fluxes is zero on average along the guiding drift contour.

Although this paragraph focuses only on the case of a magnetic field dipolarization, one can easily extend the approach to more general changes between different states of external magnetic field models. Since $\Delta L^*(\varphi) = L_{dip}^*(\varphi) - L^*$ provides direct quantification of the intensity of nonadiabatic transport, (L_{dip}^*, φ) represents a meaningful set of coordinates to track the radial motion of radiation belt particles. In addition, unlike L^* , L_{dip}^* does not require that particles be on closed drift shells; the definition of L_{dip}^* requires a closed field line only. This feature is of interest for modeling the transport of particles initially on open drift shells.

3. Derivation of the L^* Approximation

We consider a particle that moves from a point (r_0, φ_0) on the initial guiding drift contour Γ to the circular contour L^* , as the magnetic field varies adiabatically from the initial topology (denoted by the subscript i) to the dipolar state (denoted by the subscript dip). We note $B_{\text{dip}}(r, \theta_m) = k_0 f(\theta_m) / (r_0 R_e)^3$ as the dipolar magnetic field intensity at the mirror point $(r = r_0 \sin^2 \theta_m, \theta_m, \varphi)$. By definition of the dipolar magnetic field, $f(\theta_m) = \sqrt{1 + 3 \cos^2 \theta_m} \sin^{-6} \theta_m$. Since the dipolarization is very slow in comparison with the drift period, the variation of the magnetic field mirror intensity does not depend on the longitudinal position along the contour

$$\Delta B_m = \langle \Delta B_m \rangle. \quad (10)$$

Thus, starting from (r_0, φ_0) , we have

$$\frac{k_0 f(\theta_m)}{(L^* R_e)^3} - B_{m,i}(r_0, \varphi_0) = \frac{k_0 f(\theta_m)}{R_e^3} \left\langle \frac{1}{L_{\text{dip}}^*} \right\rangle^3 - \langle B_{m,i} \rangle, \quad (11)$$

where $k_0 f(\theta_m) R_e^{-3} \langle 1/L_{\text{dip}}^* \rangle^3$ is the dipolar magnetic field intensity expressed by means of the drift average operator. We approximate the drift average operator by a circular average operator $f \rightarrow \bar{f}$ defined according to the equation

$$\bar{f}(r_0) = \frac{1}{2\pi} \oint f(r_0, \varphi) d\varphi, \quad (12)$$

where the integration is performed at a constant radial distance to the position of the Earth's dipole at the minimum B surface. Accordingly, we assume that the variation of the magnetic field mirror intensity is similar to its circular average

$$\Delta B_m \cong \overline{\Delta B_m}, \quad (13)$$

thus,

$$\frac{k_0 f(\theta_m)}{(L^* R_e)^3} - B_{m,i}(r_0, \varphi_0) \cong \frac{k_0 f(\theta_m)}{R_e^3} \left(\frac{1}{L_{\text{dip}}^*} \right)^3 - \overline{B_{m,i}}(r_0). \quad (14)$$

We introduce L_0^* , the harmonic circular average of the L_{dip}^* parameters:

$$\frac{1}{L_0^*} = \overline{\left(\frac{1}{L_{\text{dip}}^*} \right)}. \quad (15)$$

Solving equation (14) for L^* , we obtain

$$L^* \cong L_0^* \left(1 + \left(\frac{L_0^*}{r_0} \right)^3 \frac{(B_{m,i}(r_0, \varphi_0) - \overline{B_{m,i}}(r_0))}{B_{\text{dip}}(r, \theta_m)} \right)^{-1/3}. \quad (16)$$

In a symmetric magnetic field, $B_{m,i}(r_0, \varphi_0) = \overline{B_{m,i}}(r_0)$ and $L^* = L_0^*$. In an asymmetric magnetic field, in a manner similar to the equations derived by Schulz [1972; equations (25), (26a), and (26b)], L_0^* is a zero-order approximation of L^* , weighted by a correction factor

$$\left(1 + \left(\frac{L_0^*}{r_0} \right)^3 \frac{(B_{m,i}(r_0, \varphi_0) - \overline{B_{m,i}}(r_0))}{B_{\text{dip}}(r, \theta_m)} \right)^{-1/3}, \quad (17)$$

which is responsible for mimicking the effects of both the asymmetry of the magnetic field and the shell splitting on the variation of L^* .

While $(B_{m,i}(r_0, \varphi_0) - \overline{B_{m,i}}(r_0)) / B_{\text{dip}}(r, \theta_m)$ is only a correction factor, its computation requires a lot of field line tracing because the magnetic field intensity at the mirror points should be iteratively searched by

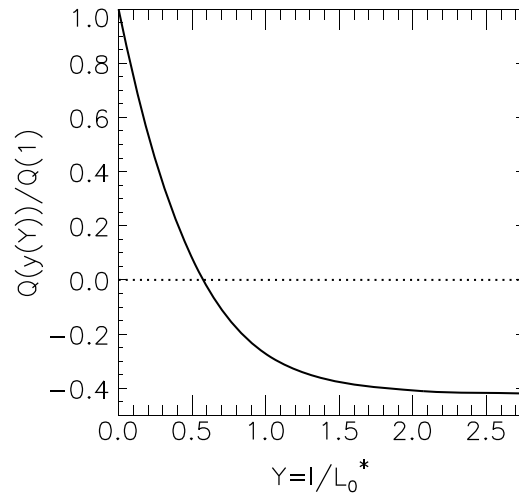


Figure 3. The $Q \circ y(Y)/Q(1)$ ratio as a function of the normalized second invariant $Y=l/L_0^*$.

conservation of the second adiabatic invariant. To avoid this problem, we take advantage of the shell splitting factor introduced by Schulz [1972], and we infer that the ratio $(B_{m,i}(r_0, \varphi_0) - \overline{B_{m,i}}(r_0))/B_{\text{dip}}(r, \theta_m)$ is proportional to the one computed at the minimum B surface:

$$\frac{(B_{m,i}(r_0, \varphi_0) - \overline{B_{m,i}}(r_0))}{B_{\text{dip}}(r, \theta_m)} = \frac{Q(y)}{Q(1)} \frac{(B_{0,i}(r_0, \varphi_0) - \overline{B_{0,i}}(r_0))}{B_{\text{dip}}(r_0, \pi/2)}, \quad (18)$$

where $B_{0,i}$ is the intensity of the initial magnetic field at the minimum B surface (subscript 0) and $y = \sin \alpha$ is the sine of the equatorial pitch angle in the dipole magnetic field.

Following Schulz, we set

$$Q(y) = \frac{37Y(y) - 42T(y) + F(y)}{21(6T(y) - Y)}, \quad (19)$$

where the functions Y , T , and F are given, respectively, in equations (4), (11a), and (22c) in Schulz' [1972] paper.

The function Y relates to the second invariant via $Y=J/(2pL_dR_e)$, where p is the scalar momentum and $L_d \equiv \lim_{\theta \rightarrow 0} (r/(R_e \sin^2 \theta))$. In order to relate $y \mapsto Q(y)$ to quantities computable in the initial magnetic field, we

assume that $Y(y) \cong l/L_0^*$, with $l = \int_{s_m}^{s_m'} \sqrt{1 - B(s)/B_m} ds$, and we change the variable y to the variable Y in equation (19). A curve fitting of the Q ratio as a function of Y gives the following approximation

$$\begin{aligned} \frac{Q \circ y(Y)}{Q(1)} \cong & -0.0085 \cdot Y^6 + 0.0599 \cdot Y^5 - 0.0667 \cdot Y^4 - 0.5039 \cdot Y^3 \\ & + 1.9124 \cdot Y^2 - 2.6662 \cdot Y + 1. \end{aligned} \quad (20)$$

This function is illustrated Figure 3.

Putting equation (20) into equation (16), one can write

$$L^*(r_0, \varphi_0 Y) \cong L_0^*(r_0) \left(1 + \frac{Q \circ y(Y)}{Q(1)} \left(\frac{L_0^*(r_0)}{r_0} \right)^3 \frac{(B_{0,i}(r_0, \varphi_0) - \overline{B_{0,i}}(r_0))}{B_{\text{dip}}(r_0, \pi/2)} \right)^{-1/3}. \quad (21)$$

In the case of a weakly asymmetric field model,

$$\left(\frac{L_0^*(r_0)}{r_0} \right)^3 \frac{(B_{0,i}(r_0) - \overline{B_{0,i}}(r_0))}{B_{\text{dip}}(r_0, \pi/2)} \ll 1, \quad (22)$$

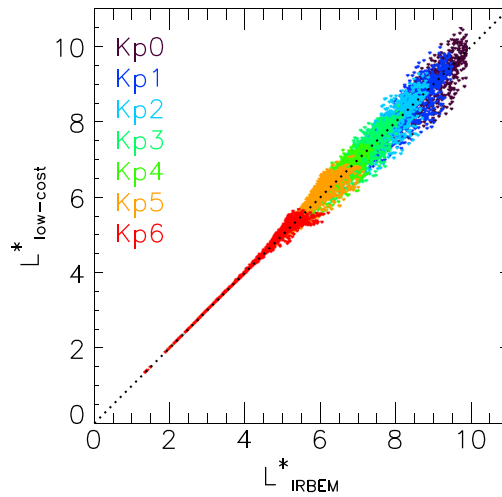


Figure 4. A comparison of the low-cost L^* approximation with the L^* parameter evaluated by the IRBEM library for different Kp indexes.

and the equation (21) becomes

$$L^*(r_0, \varphi_0, Y) \cong L_0^*(r_0) \left(1 - \frac{1}{3} \frac{Q \circ y(Y)}{Q(1)} \left(\frac{L_0^*(r_0)}{r_0} \right)^3 \frac{(B_{0,i}(r_0, \varphi_0) - \overline{B_{0,i}(r_0)})}{B_{\text{dip}}(r_0, \pi/2)} \right). \quad (23)$$

The shell splitting coefficient $-Q \circ y(Y)/3Q(1)$ ranges continuously from $-Q(1)/3Q(1) \cong -0.33$ to $-Q(0)/3Q(1) \cong 0.15$ as the equatorial pitch angle decreases from 90° to 0° , just as in Schulz' [1972; equations (25), (26a), and (26b)] paper.

4. Implementation and Performance of the "Low-Cost" L^* Algorithm

We perform a numerical study to investigate the range of validity of equation (21). The test has been carried out in a cube centered in the origin in the geographic coordinate system, with the x , y , and z coordinates ranging from $-12 R_e$ to $12 R_e$, with a $1 R_e$ increment for the seven different Kp states of the T89 model. We select the International Geomagnetic Reference Field and the eccentric tilted dipole model as internal magnetic field models to evaluate L^* with the International Radiation Belt Environment Modeling library (IRBEM-LIB) and with the low-cost algorithm, respectively.

4.1. Implementation

L^* is processed as follows:

1. During a preparation step, the circular averages $L_0^* = 2\pi / \oint \sin^2 \theta_e(r_0, \varphi) d\varphi$ and $\overline{B_{0,i}(r_0)} = \oint B_{0,i}(r_0, \varphi) d\varphi / 2\pi$ are computed for a suitable range of r_0 and various suitable external magnetic field models (i.e., various Kp values in the case of T89).

Then,

2. Starting from a point \mathbf{r} in space, the local mirror magnetic field $B_m(\mathbf{r})$ is stored.
3. The magnetic field line passing through \mathbf{r} is followed until the magnetic equator \mathbf{r}_0 of the field line is found. We determine the distance r_0 between the magnetic equator \mathbf{r}_0 and the center of the Earth's dipole, and the local equatorial magnetic field $B_{0,i}(r_0, \varphi_0)$ is stored.
4. The field line tracing is carried on until finding the mirror point whose magnetic field intensity is $B_m' = B_m(\mathbf{r})$.

The invariant $I = \int_{s_m}^{s_m'} \sqrt{1 - B(s)/B_m} ds$ is computed.

5. From \mathbf{r}_0 , the parameters L_0^* , $\overline{B_{0,i}(r_0)}$, and $B_{\text{dip}}(r_0, \pi/2) = k_0/(r_0 R_e)^3$ are calculated.
6. From $I/L_0^* = Y$, the $Q \circ y(Y)/Q(1)$ function is evaluated following equation (20).
7. Finally, L^* is calculated according to equation (21).

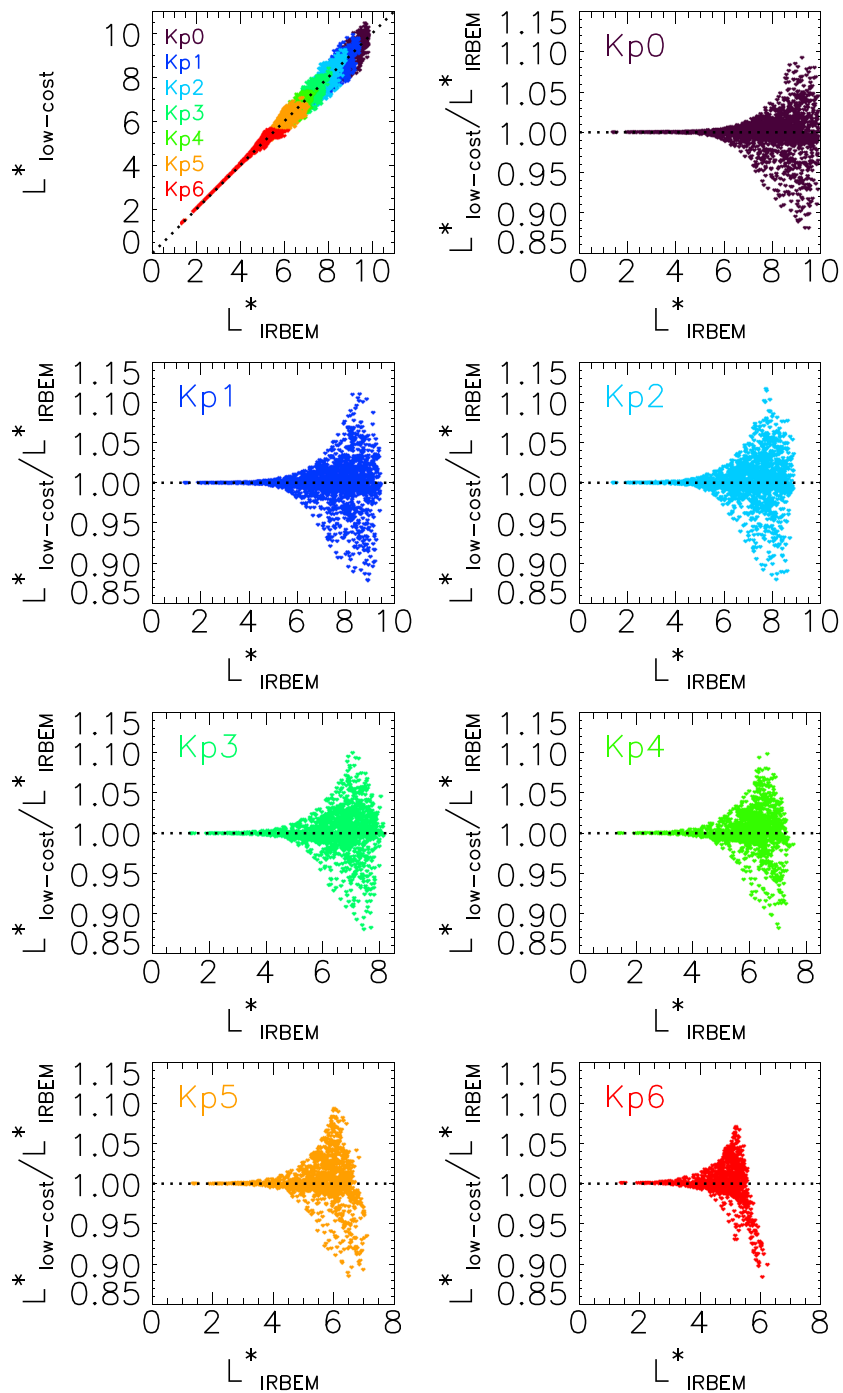


Figure 5. Ratios between the low-cost L^* evaluations and the L^* parameters derived by the IRBEM library as a function of the L^* parameter and the Kp index.

In comparison to other attempts to lower the computational price of L^* , the low-cost method is an approximate method which does not require any drift shell tracing, and circular averages are computed instead. When performed, the preparation step of the low-cost method consists of the computation of two one-dimensional tables ($r_0 \mapsto L_0^*$ and $r_0 \mapsto \overline{B_{0,j}}(r_0)$) for each magnetic field model chosen, and no iterative search approach is to be carried out. Finally, the effects of the asymmetry of the magnetic field and the shell splitting on the variation of L^* are approximated analytically so as to restrict field line tracing operations to the tracing of the initial magnetic field line between mirror points only.

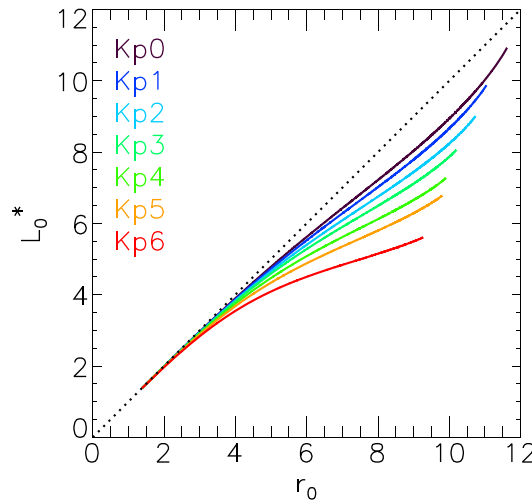


Figure 6. L_0^* as a function of the equatorial distance r_0 for different Kp indexes.

while neglecting the effects of both the asymmetry of the field and the shell splitting. Due to its simplicity, we also investigated the range of validity of L_0^* as a coarse L^* approximation. Figure 6 gives L_0^* as a function of r_0 for different Kp indexes. Figure 7 shows the comparison of L_0^* with L^* evaluated with the IRBEM-LIB. As expected, L_0^* corresponds to L^* in the symmetric region of the inner magnetosphere, for $L^* \leq 4$. Then, the relative difference $|L_0^* - L^*|/L^*$ increases until reaching a substantial factor of 20% near $L^* = 10$. In Figure 8, we present the histogram plot of the relative differences between L_0^* and L^* given by the IRBEM-LIB superimposed over the histogram of the relative differences between the low-cost L^* approximations and the L^* given by the IRBEM-LIB (in blue).

In order to compare the result of this algorithm with the L_m parameter introduced by McIlwain [1961], we define the skill score parameter $sk(r, Kp)$ according to the relation

$$sk(r, Kp) = 1 - \frac{|L_{low\ cost}^* - L_{IRBEM}^*|}{|L_m - L_{IRBEM}^*|} \tag{24}$$

The skill score is negative when L_m provides a better estimation of L^* than $L_{low\ cost}^*$ and it is positive when $L_{low\ cost}^*$ provides a better estimation of L^* than L_m . When the margins of errors of the two approximations

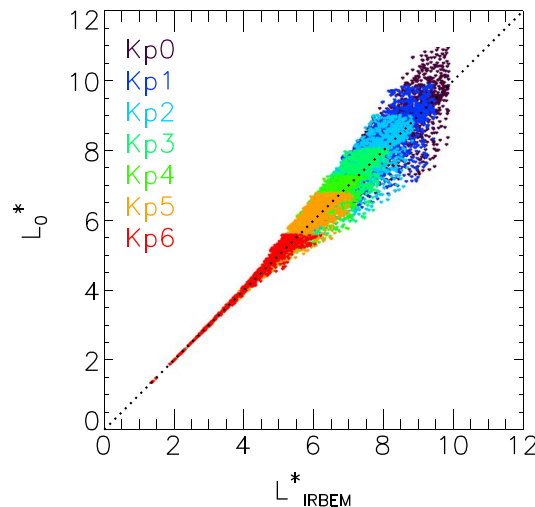


Figure 7. A comparison of the L_0^* parameter with the L^* parameter evaluated by the IRBEM library for different Kp indexes.

4.2. Performance

The results are presented in Figure 4. The ratios between the L^* approximation and the L^* obtained with the IRBEM-LIB are displayed in Figure 5 as a function of L^* and Kp . We obtain a speedup of almost 3 orders of magnitude and a relative difference which increases up to 12% for the largest L^* parameters, i.e., a difference of 1.2 at $L^* \approx 10$ for a Kp index equal to 0 in the worst case.

A study of the relative difference as a function of the $I/I_0^* = Y$ parameter has also been performed. It shows no dependence of the performance of the algorithm with the distance to the magnetic equator, or equivalently, with the pitch angle.

L_0^* gives a zero-order approximation of L^* as a function of the equatorial distance r_0 only

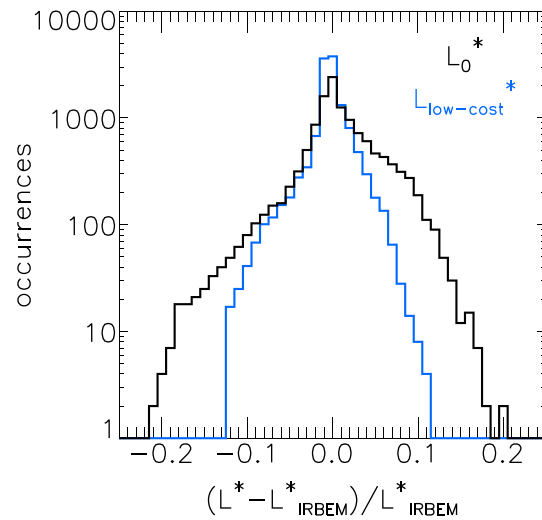


Figure 8. Histogram plot of the relative differences between the L_0^* and the L^* parameters evaluated with the IRBEM library (in black) and the relative differences between the low-cost L^* approximations and the L^* parameters evaluated with the IRBEM library (in blue).

are equal, then $sk(r, Kp) = 0$. $sk(r, Kp) = 1$ when $L^*_{low\ cost}$ performs infinitely better than L_m for approximating L^* . The averages of the skill scores as a function of the Kp index are given in Table 1.

Negative skill scores are obtained for the Kp indexes equal to 0 or 1 only, at large distances ($r_0 \geq 7.5$), within approximately 25° to the magnetic equator. In comparison with L_m , the low-cost L^* provides a better approximation of L^* in 98% of cases. In addition, L_0^* provides a better approximation of L^* than L_m in 93.5% of cases.

In practice, we suggest that the user set a margin of acceptable error and define the range of validity for the low-cost L^* algorithm accordingly referring to Figure 5. Within this range of validity, the low-cost method can be preferred to any other method in order to provide a fast, accessible, and reasonable evaluation of L^* . Beyond this range of validity, more refined methods should be used.

5. Conclusions

In this paper, we have worked with the magnetic colatitudes of field line foot points computed in magnetic field models assuming the internal dipole magnetic field. We have shown that we can visualize and evaluate the topological variation of a given magnetic field model from the dipolar state using these colatitude coordinates, and we have introduced the L_{dip}^* parameter as a field line label. We have proven that L^* can be defined as the harmonic drift average of the L_{dip}^* parameters of the bunch of field lines constituting the shell. We have then derived an L^* approximation from the description of the variation of the magnetic field mirror intensity after an adiabatic dipolarization considering that the drift average operator is comparable to the circular drift average operator. Based on this approximation, we have suggested an algorithm which calculates L^* from the real-time sampling of a magnetic field line between mirror points only. This algorithm is fast, because it does not require a computationally expensive drift contour tracing, and it is accessible, because it consists only of a few steps applicable in any external magnetic field model, given in section 4.1. The relative difference between the result obtained and the result given by the IRBEM-LIB increases up to 12% for the largest L^* parameters, in the case of the T89 model for the external magnetic field. This relative difference is similar to the margin of error due to small deviations between magnetic models at geosynchronous orbit. Therefore, we believe that this low-cost algorithm provides a reasonable compromise between computational speed and accuracy of particular interest for real-time space weather forecast purposes.

Table 1. Average Skill Scores as a Function of the Kp Index

Kp	0	1	2	3	4	5	6
$sk(Kp)$	0.70	0.83	0.89	0.92	0.94	0.95	0.96

Acknowledgments

The author acknowledges financial support from the Natural Environment Research Council. She is grateful to Richard B. Horne who has encouraged this work and has taken the time to comment critically on the draft of this paper. She is also grateful to Juan G. Roederer for the valuable discussions and comments. IRBEM-LIB can be downloaded at <http://sourceforge.net/projects/irbem/>.

Larry Kepko thanks James McCollough and another reviewer for their assistance in evaluating this paper.

References

- Bedingfield, K. L., R. D. Leach, and M. B. Alexander (1996), *Spacecraft System Failures and Anomalies Attributed to the Natural Space Environment*, NASA Reference Publication 1390, National Aeronautics and Space Administration Marshall Space Flight Center, MSFC, Ala.
- Beutier, T., and D. Boscher (1995), A three-dimensional analysis of the electron radiation belt by the Salammbô code, *J. Geophys. Res.*, *100*, 14,853–14,861, doi:10.1029/94JA03066.
- Birmingham, T. J., and F. C. Jones (1968), Identification of moving magnetic field lines, *J. Geophys. Res.*, *73*, 5505–5510, doi:10.1029/JA073i017p05505.
- Boscher, D., S. Bourdarie, P. O'Brien, and T. Guild (2012), IRBEM Library, Version 4.4.0.
- Fälthammar, C., and F. S. Mozer (2007), On the concept of moving magnetic field lines, *Eos Trans. AGU*, *88*, doi:10.1029/2007EO150002. Issn:0096-3941.
- Fillius, R. W., and C. E. Mcllwain (1967), Adiabatic betatron acceleration by a geomagnetic storm, *J. Geophys. Res.*, *72*, 4011–4015, doi:10.1029/JZ072i015p04011.
- Glauert, S. A., R. B. Horne, and N. P. Meredith (2013), Three dimensional electron radiation belt simulations using the BAS Radiation Belt Model with new diffusion models for chorus, plasmaspheric hiss and lightning-generated whistlers, *J. Geophys. Res. Space Physics*, *119*, 268–289, doi:10.1002/2013JA019281.
- Horne, R. B., S. A. Glauert, N. P. Meredith, D. Boscher, V. Maget, D. Heynderickx, and D. Pitchford (2013), Space weather impacts on satellites and forecasting the Earth's electron radiation belts with SPACECAST, *Space Weather*, *11*, 169–186, doi:10.1002/swe.20023.
- Huang, C.-L., H. E. Spence, H. J. Singer, and N. A. Tsyganenko (2008), A quantitative assessment of empirical magnetic field models at geosynchronous orbit during magnetic storms, *J. Geophys. Res.*, *113*, A04208, doi:10.1029/2007JA012623.
- Koller, J., and S. Zaharia (2011), LANL* V2.0: Global modeling and validation, *Geosci. Model. Dev.*, *4*, 669–675, doi:10.5194/gmd-4-669-2011.
- Koller, J., G. D. Reeves, and R. H. W. Friedel (2009), LANL* V1.0: A radiation belt drift shell model suitable for real-time and reanalysis applications, *Geosci. Model. Dev.*, *2*, 113–122, doi:10.5194/gmd-2-113-2009.
- Koons, H. C., J. E. Mazur, R. S. Selesnick, J. B. Blake, J. F. Fennell, J. L. Roederer, and P. C. Anderson (2000), The impact of the space environment on space systems, 6th Spacecraft Charging Technology Conference, AFRL-VS-TR-20001578.
- McCollough, J. P., J. L. Gannon, D. N. Baker, and M. Gehmeyr (2008), A statistical comparison of commonly used external magnetic field models, *Space Weather*, *6*, S10001, doi:10.1029/2008SW000391.
- Mcllwain, C. E. (1961), Coordinates for mapping the distribution of magnetically trapped particles, *J. Geophys. Res.*, *66*, 3681–3691, doi:10.1029/JZ066i011p03681.
- Min, K., J. Bortnik, and J. Lee (2013a), A novel technique for rapid L^* calculation using UBK coordinates, *J. Geophys. Res. Space Physics*, *118*, 192–197, doi:10.1029/2012JA018177.
- Min, K., J. Bortnik, and J. Lee (2013b), A novel technique for rapid L^* calculation: Algorithm and implementation, *J. Geophys. Res. Space Physics*, *118*, 1912–1921, doi:10.1002/jgra.50250.
- National Research Council (2008), *Severe Space Weather Events—Understanding Societal and Economic Impacts: A Workshop Report*, The National Academies Press, Washington, D. C.
- Newcomb, W. A. (1958), Motion of magnetic lines of force, *Ann. Phys.*, *3*, 347–385, doi:10.1016/0003-4916(58)90024-1.
- Roederer, J. G. (1967), On the adiabatic motion of energetic particles in a model magnetosphere, *J. Geophys. Res.*, *72*(3), 981–992, doi:10.1029/JZ072i003p00981.
- Roederer, J. G. (1970), *Dynamics of Geomagnetically Trapped Radiation*, Springer, New York, doi:10.1007/978-3-642-49300-3.
- Roederer, J. G. (1972), Geomagnetic field distortions and their effects on radiation belt particles, *Rev. Geophys.*, *10*(2), 599–630, doi:10.1029/RG010i002p00599.
- Roederer, J. G., and H. Zhang (2014), Particle fluxes, distribution functions and violation of invariants, in *Dynamics of Magnetically Trapped Particles, Foundations of the Physics of Radiation Belts and Space Plasmas*, Astrophysics and Space Science Library, vol. 403, chap. 4, Springer-Verlag, Berlin, Heidelberg, doi:10.1007/978-3-642-41530-2.
- Schulz, M. (1972), Drift-shell splitting at arbitrary pitch angle, *J. Geophys. Res.*, *77*, 624–634, doi:10.1029/JA077i004p00624.
- Schulz, M. (1991), The Magnetosphere, *Geomagnetism*, *4*, 88–293.
- Stern, D. P. (1994), The art of mapping the magnetosphere, *J. Geophys. Res.*, *99*, 17,169–17,198, doi:10.1029/94JA01239.
- Tsyganenko, N. A. (1989), A magnetospheric magnetic field model with a warped tail current sheet, *Planet. Space Sci.*, *37*(1), 5–20.
- Tsyganenko, N. A. (1995), Modeling the Earth's magnetospheric magnetic field confined within a realistic magnetopause, *J. Geophys. Res.*, *100*, 5599–5612, doi:10.1029/94JA03193.
- Tsyganenko, N. A., and M. I. Sitnov (2005), Modeling the dynamics of the inner magnetosphere during strong geomagnetic storms, *J. Geophys. Res.*, *110*, A03208, doi:10.1029/2004JA010798.
- Tsyganenko, N. A., and M. I. Sitnov (2007), Magnetospheric configurations from a high-resolution data-based magnetic field model, *J. Geophys. Res.*, *112*, A06225, doi:10.1029/2007JA012260.
- Ukhorskiy, A. Y., M. I. Sitnov, R. M. Millan, B. T. Kress, and D. C. Smith (2014), Enhanced radial transport and energization of radiation belt electrons due to drift orbit bifurcations, *J. Geophys. Res. Space Physics*, *119*, 163–170, doi:10.1002/2013JA019315.
- Whipple, E. C. (1978), (U,B,K) coordinates: A natural system for studying magnetospheric convection, *J. Geophys. Res.*, *83*, 4318–4326, doi:10.1029/JA083iA09p04318.
- Yu, Y., J. Koller, S. Zaharia, and V. Jordanova (2012), L^* neural networks from different magnetic field models and their applicability, *Space Weather*, *10*, S02014, doi:10.1029/2011SW000743.

Erratum

In the originally published version of this article, in the Acknowledgments, the wrong editor name was listed. This error has since been corrected, and this version may be considered the authoritative version of record.